Lawrence Berkeley National Laboratory

Lawrence Berkeley National Laboratory

Title

Auto-oligomerization and hydration of pyrrole revealed by x-ray absorption spectroscopy

Permalink

https://escholarship.org/uc/item/1cg5g643

Author

Schwartz, Craig P.

Publication Date

2009-09-21

Peer reviewed

Auto-Oligomerization and Hydration of Pyrrole Revealed by X-ray Absorption Spectroscopy

Craig P. Schwartz[1,2], Janel S. Uejio[1,2], Andrew M. Duffin[1,2], Alice H. England[1,2], David Prendergast[3], Richard J. Saykally[1,2]*

1. Department of Chemistry, University of California, Berkeley

2. Chemical Sciences Division, Lawrence Berkeley National Laboratory

3. Molecular Foundry, Lawrence Berkeley National Laboratory

* Corresponding Author - E-mail: saykally@berkeley.edu

Phone : (510) 642-8269

Fax : (510) 642-8566

Abstract

Near edge x-ray absorption fine structure (NEXAFS) spectra have been measured at the carbon and nitrogen K-edges of the prototypical aromatic molecule, pyrrole, both in the gas phase and when solvated in water, and compared with spectra simulated using a combination of classical molecular dynamics and first principles density functional theory in the excited state core hole approximation. The excellent agreement enabled detailed assignments. Pyrrole is highly reactive, particularly in water, and reaction products formed by the auto-oligomerization of pyrrole are identified. The solvated spectra have been measured at two different temperatures, indicating that the final states remain largely unaffected by both hydration and temperature. This is somewhat unexpected,since the nitrogen in pyrrole can donate a hydrogen bond to water.

1. **Introduction**

Only slightly soluble (47 g/L) in water,[1] pyrrole is a very weak base due to the partial delocalization of its nitrogen lone pair electrons. It reacts via electrophilic substitution and oligomerizes readily upon contact with light or air.[2] As a heterocyclic aromatic component of important macrocycles, including hemes and chlorophyll, it is an important prototype for detailed study. Here, we investigate pyrrole using X-ray absorption spectroscopy (XAS) experiments and a promising new theoretical formalism, seeking to explore the agreement between theory and experiment, anticipating future studies of similar, but more complex molecules.

The development of near edge X-ray absorption fine structure spectroscopy (NEXAFS) of liquid microjets has provided a useful new tool for characterizing the details of solvation.[3] NEXAFS probes the unoccupied molecular orbitals, which are highly sensitive to intermolecular interactions.[4,5] This new approach to the study of liquids is yielding important insights into the behavior of aqueous systems, but the chemical information that can be extracted from the measurements is currently limited by the available theoretical methods for computing core-level spectra. Here, we use the newly-developed excited core hole (XCH) method, which allows for accurate calculations of XAS spectra. This study provides a good test of the ability of XCH to describe highly delocalized bonding systems, which are problematic for the methods now commonly used.

NEXAFS spectra of water differ greatly upon changing from solid to liquid to gas,[5,6] as do those of glycine when comparing the solid and gaseous forms to the form solvated in water.[3,7] However, these molecules exhibit strong intermolecular interactions either via hydrogen bonding or by modifying of their charge state, so large spectral changes are expected. In both microwave

and theoretical studies of clusters comprising one pyrrole and one water molecule, the N-H group appears to interact exclusively with the water, preventing water from interacting with the ring.[8,9] It has been known for some time that the vibrational spectrum of the N-H bond of pyrrole is red-shifted when dissolved in liquid water versus when in neat solution.[10] Both these results imply that the N-H group has strong intermolecular interactions with liquid water. This makes pyrrole an interesting case, because the ring carbons of pyrrole should interact with water in a manner similar to those of benzene, whereas the N-H group can interact strongly. It was previously thought that hydrophobic solvation involved generating "icebergs" in water because the hydrophobic solute would structure the water.[11] This is no longer believed to be the case, as deduced largely from classical molecular dynamics simulations.[11,12] However, such simulations are incapable of describing detailed quantum effects, such as the extent of orbital mixing between pyrrole and water, for which NEXAFS is a sensitive probe.[13] Previous study of pyrrole has shown that its solid form has very similar NEXAFS spectra to the inner shell electron energy loss spectroscopy (ISEELS) measurements of pyrrole in the gas phase.[14-17] This implies that in the solid, the orbitals of pyrrole do not exhibit significant hybridization.

Pyrrole is known to be very reactive, and previous studies have observed particles of micron size in liquid pyrrole.[18] It polymerizes readily in the presence of a platinum electrode[19] and has important autopolymerization properties for controlling the growth and properties of gold nanoparticles.[20] In fact, neat pyrrole is known to oligomerize readily when exposed to either air or light.[2] However, it will not react if exposed to neither. Unfortunately, under realistic conditions, pyrrole suffers exposure to stray light and air, leading to impure samples over time.[21] This process is accelerated in water at neutral pH. It is believed that in pH-neutral water, the oligomerization proceeds by dimerizing, which, if then repeated many times, would

produce the polymer.[22] This reactivity of pyrrole is important for X-ray absorption studies because, unlike in vibrational spectroscopy, spectral features resulting from reaction products will overlap with the pure pyrrole spectrum.

There are several methods of obtaining high-resolution X-ray absorption spectra of liquids; in our case small jets of water solutions (~30 microns) were windowlessly coupled to a synchrotron beamline. An advantage of this method is that the liquid is not affected by interactions with silicon nitride windows; this is useful, as we want to probe the nitrogen K-edge. Additionally, the solution is constantly renewed, thereby avoiding sample damage.[23] One of the biggest advantages is that the temperature can be easily controlled by allowing the liquid to evaporatively cool.[24] Furthermore, one can easily obtain a sample of the vapor, enabling a direct comparison of liquid and gas spectra.

In order to model the pyrrole spectra, density functional theory (DFT) is used within the generalized gradient approimxation (GGA).[25] DFT has exhibited reasonable accuracy in reproducing core level spectra via total energy differences (ΔSCF or ΔKS).[26] There are several methods of calculating NEXAFS spectra,[27,28] but we choose to model our system using a full core hole and the associated lowest energy excited electron (XCH).[29,30] We represent the electronic structure using plane waves, because they can accurately describe scattering states that are often found above the ionization potential and can accurately describe localized band excited states, as well as spatially extended Ryberg-like states. Linear combinations of atomic orbitals are often inadequate for describing such extended states.[28] We approximate the high energy continuous electron density of states by using periodic boundary conditions and numerically converging an integration over the first Brillouin zone (BZ). For extended states that span the supercell, an accurate determination of the electronic density of states can be achieved by such

BZ sampling.[31] We simulated the atomic configurations of pyrrole both in the gas phase and aqueous solution with classical molecular dynamics. This method has the advantage of capturing the impact of nuclear motion on the electronic transition amplitude.[32] We note that the same techniques have been applied successfully to interpreting the spectra of solvated amino acids.[33]

2. Methods

2.1 Samples: Pyrrole was obtained commercially from Sigma-Aldrich, with stated purities of at least 98%. All water used had a resitivity of 18 MΩ/cm. Samples were used without further purification. The pH of the solution was approximately 7 and the molecule is expected to be predominantly neutral at this pH.[34] The pK_{aH} of pyrrole is approximately -4. The concentration of the solution used was ~0.5 M. We note that the sample was not fresh and may have undergone oligomerization prior to our use.

2.2 NEXAFS Spectroscopy of Solvated and Gaseous Pyrrole: Total electron yield (TEY) X-ray absorption spectra (XAS) were recorded at the carbon K-edge (~300 eV) and nitrogen K-edge (~400 eV). These measurements were performed at Beamline 8.0.1 of the Advanced Light Source (ALS) at Lawerence Berkeley National Laboratory in Berkeley, CA. A detailed description of the experimental system has been published previously.[23] Briefly, an intense (> 10^{11} photons/sec), high resolution (E/ΔE > 4000) tunable X-ray beam is generated from an undulator at the ALS. The synchrotron light is then focused (~50 μm spot size) onto a small liquid jet (~30 μm diameter) and the TEY is collected to obtain spectra of the bulk liquid.[5] The jet is produced by using a syringe pump (Teledyne-Isco) to pressurize the liquid behind a fused silica capillary tip. The jet travels parallel to the polarization of the incident radiation. Almost immediately (~0.5 mm and ~15 μs) after leaving the tip orifice, the liquid is intersected by the X-ray beam, wherein the sample is close to room temperature (~ 21.5°C ± 1.5°C).[24]

Additional measurements were taken downstream (2 cm), allowing the jet to evaporatively cool before being exposed to the X-ray beam. The energy step size used was 0.1 eV in all scans. The liquid jet is then condensed in a separate cryogenically cooled section of the chamber to maintain low pressures ($\sim 10^{-4}$ torr) in the interaction region. In order to collect a vapor spectrum, the jet is moved out of the X-ray beam and a spectrum of the vapor present near the jet is taken.

This approach provides several advantages over other emergent methods for studying X-ray spectra of liquids. Typical pressures in the main experimental chamber are $\sim 10^{-4}$ torr, but two differential pumping sections allow the beamline to maintain UHV conditions without using windows, which would limit the flux. Furthermore, sample damage is minimized by employing this constantly renewing source. The low operating pressures permit the use of sensitive charged particle detection as a function of X-ray energy (i.e. action spectra). The TEY is detected by locating a small (~ 1 mm^2) positively biased copper electrode close (<5 mm) to the jet. The detected electron current is amplified and converted to a voltage before being read out by the beamline computer. The signal is normalized to that from a gold mesh located ~ 3 meters up-beam of the chamber. The energy is calibrated based on specific metal impurities located in the beamline optics and the spectra are area normalized.

2.3 Calculations

Core-level spectra: Our theoretical approach has been described previously.[29,32] We employ periodic boundary conditions using a plane-wave basis that is accurate for both localized and delocalized states. The zone-center electronic structure is calculated using the PWSCF code.[35] Core-hole matrix elements with valence electrons were calculated by reconstructing the core region of the excited atom of the pseudo states within the atomic frozen core approximation. Transition amplitudes are estimated in the single-particle and dipole approximations; excitations

to states above this first excited state are approximated using the unoccupied Kohn-Sham eigenstates computed from the excited core hole (XCH) self-consistent potential. We use the Perdew-Burke-Erzenhoff (PBE) form of the generalized gradient approximation to the exchange-correlation potential.[36] These calculations were performed on the Franklin supercomputer at NERSC.

Isolated Pyrrole: Large simulation cells are used $((20 \text{ Å})^3)$ to reduce spurious interactions between cells for the isolated molecule and so as to be large enough to accurately represent excited states below the ionization potential (IP). Approximately 100 Kohn-Sham eigenstates are used in constructing transition matrix elements. Due to the large box size, a large number of unoccupied states are needed in order to describe high-energy transitions.

Solvated Pyrrole: Significantly smaller cells $((\sim 13 \text{ Å})^3)$ were sufficient to reduce the spurious interactions between hydrated molecules. A single pyrrole molecule was solvated by 81 water molecules, under periodic boundary conditions. Approximately 1000 Kohn-Sham eigenstates are used to extend the spectra approximately 20 eV above the LUMO energy (absorption onset).

Molecular Geometry: Generally, core-level spectra of isolated molecules are simulated within the fixed-nuclei approximation,[26] particularly for molecules in their vibrational ground state. The lowest energy geometrical structure is determined by minimizing the forces derived from the Born-Oppenheimer Hamiltonian, a formalism which models the electrons as quantum particles and the nuclei as classical point charges. We generate spectra from this single molecular configuration on isolated pyrrole molecules and these are referred to herein as fixed-nuclei calculations.

Unfortunately this will be inadequate to properly describe the intrinsic spectral broadening, as a major source of broadening can be caused by thermally excited vibrations and zero-point motion of the molecule. These motions can lead to new transitions and large shifting of transition energies. Within the Born-Oppenheimer approximation, the effect of such motions on the transition strength is known to first order as the Herzberg-Teller effect.[37] In order to account for these effects, we have modeled the nuclear degrees of freedom in these molecules using molecular dynamics (MD) performed at 300 K using a Langevin thermostat, with the generalized AMBER force field. The resulting distribution of nuclear coordinates was sampled at 20 picosecond intervals to eliminate correlation between snapshots. This was done for 100 snapshots for both the isolated and solvated case of pyrrole.[38] These coordinates we subsequently used in DFT calculations which were by far the most significant part of the computational cost.

All calculated spectra are numerically broadened using Gaussians of 0.2 eV full width at half maximum. Others often resort to ad-hoc energy dependent broadening schemes.[39] We use this relatively small and uniform broadening with the aim of simulating and distinguishing electronic and vibrational effects explicitly, thereby arriving at a predictive computational approach.

3. Results and Discussion

Carbon K-edge

Figure 1 shows the carbon K-edge spectrum of pyrrole in the gas phase measured using both ISEELS and NEXAFS.[14,17] Five major features have been identified in the spectra (labeled 1-5). Another feature has been reported previously in ISEELS studies at approximately 300 eV;

however, the evidence for this feature, given the signal to noise ratio, is not compelling. Furthermore, this feature is not evident in the NEXAFS data, indicating that it may be due to a non-dipole transition in ISEELS. Calculations for both fixed-nuclei and MD sampled spectra are shown for comparison. Carbon 1 (C1) refers to the two identical carbon atoms bound only to other carbon atoms, whereas carbon 2 (C2) refers to the two carbon atoms bound directly to the nitrogen atom of pyrrole. The fixed-nuclei spectra are dotted lines, while the average of 100 MD snapshots is shown as the solid line, with a shading indicating one standard deviation. Calculated spectra were aligned to the experimental IP of C2, 290.8 eV.[14,17] The relative alignment of C1 and C2 is obtained by total energy differences.[32] The first feature was originally believed to comprise two transitions, however, higher resolution spectra[17] and our high resolution NEXAFS clearly show this feature to comprise at least three transitions. The first two transitions within Feature 1, centered at 285.7 and 286.2 eV, respectively, have been assigned as $1sC1 \rightarrow 1\pi^*(3b_1)$ and $1sC2 \rightarrow 1\pi^*(3b_1)$. This is confirmed by our most recent theoretical calculations. The difference in peak positions corresponds to the difference in XPS binding energy of 1.0 eV between the two carbons. The molecular motions of the molecule substantially broaden these features in theoretical calculations. In the case of carbon 1, the feature is also substantially red shifted by motions of the molecule. The underestimation of the bandwidth in DFT leads to spectra which appear contracted with respect to experiment.[29] The third segment of Feature 1, visible as a shoulder at approximately 287.1 eV, has previously been assigned to a combination of a π^*/σ^* orbital transition from carbon 1;[17] however, our DFT calculations did not reproduce this feature with adequate intensity. The shift is too large to be caused by vibrations; our hypothesis is that this feature arises from chemical impurities. We did witness the same transitions observed in previous calculations, but as in previous calculations the intensity is too

weak to explain the observed intensity.[17]   This will be discussed in more detail later. Feature 2 was previously assigned to a feature from C2, primarily involving a π^* transition, in agreement with our calculations. Feature 3 was never observed experimentally before, but was predicted by earlier calculations.[17]   Our calculations indicate that it is due to a superposition of transitions, some of which involve σ^* orbitals. It is primarily C2 that causes this feature; however, much of the associated background intensity appears to come from C1. Features 4 and 5 are due to both carbons and have been assigned as due to $\sigma^*(C\text{-}N)$ and $\sigma^*(C\text{-}C)$ respectively.[14,17]   They are clearly scattering features, and one of the advantages of a plane wave basis set is the ability to capture such scattering phenomena.   Gaussian orbital calculations would have difficulty reproducing either feature.

All of the principal observed spectral features are captured, except for a shoulder of Feature 1. Our DFT calculations indicate that there are two types of transitions in this energy range.   Their assignment is in agreement with previous configuration interaction quantum chemical calculations.[17]   However, the spectral intensity of these features is insufficient to reproduce the observed shoulder of Feature 1. Higher level GW-corrected DFT calculations (not shown) were unable to reproduce the shoulder, and clearly, even with the inclusion of molecular motions, we were unable to reproduce this feature within DFT (Figure 1). This indicates that pyrrole is somehow different from isoelectronic furan, whose shoulder region can be more accurately reproduced by electronic structure calculations.[40]

Thus there must be some other cause for the peak intensity. We ruled out the possibility of pyrrole-pyrrole self interactions by examining the nonbonded dimer, consisting of two weakly interacting pyrroles.[41]   Calculations indicate that, if present, this complex does not provide sufficiently intense signal in the shoulder region (~287.1 eV), as is shown in Figure 2.

11

There is literature precedent indicating the dimerization of pyrrole in aqueous solutions, so this possibility was investigated.[2,22]   It should be noted that this process can occur merely upon exposure to light or air.[21] We believe that the pyrrole used in this study reacted while stored in a bottle.   If our interpretation is correct, this likely has happened as well in previous pyrrole studies.[17] Our pyrrole sample likely further reacted when placed in water. For this reason, much of the dimer may actually have been present before being added to water. When two pyrrole molecules are chemically bonded, as is shown at the top of Figure 2, a strong shoulder develops on Feature 1. In its lowest energy conformation, the dimer is planar, but thermal excitations at room temperature should enable dihedral angles between the rings of up to ~15˚. The shoulder increases in intensity as the molecule is twisted. The shoulder is due primarily to the carbons which bond upon dimerizing, labeled α in Figure 2. The spectra of the trimer, as well as polypyrrole, were also calculated in their vibrational ground states (within the fixed-nuclei approximation). The trimer consists of another pyrrole ring binding to the dimer via the α carbons, which could form due to subsequent reactions of the dimer in water. If the process were continually repeated, the polymer would be formed. As the oligomer chain grows longer, the shoulder region grows more intense, primarily due to the carbons bonding to other pyrrole rings. Due to this strong feature emerging in oligomerized pyrroles, we can reliably ascribe the shoulder found in the NEXAFS and ISEELS spectra to chemically bonded pyrrole.   We note that this feature may not be caused solely by water. In earlier work in which pyrrole was not dissolved in water, a similar, albeit slightly less intense, shoulder was seen.[17] It is likely that the chemical species which make up the shoulder can form in pure liquid pyrrole but will react even more rapidly when exposed to liquid water.

For illustrative purposes, we show in Figure 3 that when the planar dimer is combined with the monomer in a 1:1 ratio, all the observed low energy features are obtained. In reality, mixture of chain lengths of pyrrole oligomers would probably be present, as would more extensive molecular motions, which were not sampled here. Therefore, we are unable to determine the fraction of pyrrole that actually oligomerized. Our spectra should not be considered as quantitative, but merely as an explanation of the origin of the shoulder to Feature 1. We note that this result indicates a significant presence of oligomers. An oligomer free sample will require maintaining an air- and light-free environment after purifying the pyrrole. However, for studies under aqueous solvation oligomerization is likely unavoidable due to reactions with water.

Figure 4 displays two experimental carbon K-edge spectra of fully solvated pyrrole taken at different temperatures, and theoretical calculations for the associated carbons, with error bars corresponding to one standard deviation. The spectra look quite similar to that of the gas phase molecule, and there is only a minor temperature dependence. (Similar to the gas phase spectra, the shoulder at 287.1 eV is found here as well). In particular, the most intense part of the first feature grows slightly with an increase in temperature. This would indicate that there is less motion of the molecule at higher temperature. We believe this should be unlikely, and it is likely due at least partially to normalizing over a temperature range that is too small. It is likely that there is extra intensity outside of the temperature range relative to the low temperature spectra due to shifting of EXAFS peaks. This would cause the corresponding low energy peaks to shrink in intensity. Detector drift may also be a factor. The first feature is red-shifted by ~0.1 eV at lower temperature, but the measurement step size was also 0.1 eV so this shift cannot be quantitatively determined. This shift in energy would likely correspond to a slight change in

solvation, as the change in oligomerization should be minor between these two temperatures. At higher temperature the water will likely solvate pyrrole slightly differently than at lower temperature. Feature 3 disappears in the spectrum taken at ~295 K, but reappears to a small extent upon cooling to 275 K. This may be due to increasing gas phase pyrrole background as one moves farther down the jet. The overall spectrum remains largely invariant over the ~20˚ C temperature range.

Comparing the liquid spectra measured at 295K to the calculated liquid spectra, one reproduces the correct number and location of features, and generally the proper form of the spectra. Feature 1 still lacks the observed shoulder, since auto-oligomerization was not included in the solvated simulations, and Feature 3 disappears in the simulated spectra, as found experimentally. The calculations correctly predict the blue-shift of the large 4th feature relative to that of the gas phase spectrum. By including a large number of unoccupied states in the solvated calculations, the fifth feature could also be accurately reproduced. This was not done in the gas phase calculations and therefore the fifth feature was not as well resolved for that case. When the calculated solution phase spectra are aligned with the calculated gas phase spectra, there is remarkably little difference between the two. Feature 3 disappears, Feature 1 broadens slightly, and Feature 4 blue shifts upon condensation. We speculate that the changes to Feature 4 arise from the fact that the scattering states of the isolated molecule must be orthogonal to surrounding water states when solvated, thereby increasing their kinetic energy.

We note that we have not calculated the spectra of the oligomerization products of pyrrole in water due to computational expense. However, given the large similarity between the calculated spectra of pyrrole in the liquid and the gas we feel we can assume that the spectral change upon the products of auto-oligomerization are roughly identical both spectrally and in

14

ratio as compared to the gas. This is not surprising in that the gas is sampled directly off the evaporating liquid, and thus should be similar in composition. The reaction should occur in the liquid, although due to the large time the liquid must rest in the pump before it can be sampled, it is extremely difficult to estimate time scale of this reaction.

The carbon K-edge spectrum of solid pyrrole has previously been measured.[15] Unfortunately, the resolution of that experiment was quite low (0.8 eV), and for this reason, it is difficult to discern changes due to solidification of the pyrrole and those due simply to the low resolution of the experiment. However, the spectrum is extremely similar to the gas phase ISEELS data (Feature 1 can be described by two Gaussians, unlike the higher resolution NEXAFS data); Feature 3 would not be visible due to the low resolution. Features 2, 4 and 5 are similar to the ISEELS data. The full width at half maximum of the first feature in the solid is similar to that of the gas phase ISEELS data. We note that the solid may have contained chemical impurities as well.

The effects of solvation on the carbon K-edge NEXAFS spectra of pyrrole are relatively minor, comprising a small shift in location of a σ^* feature (feature 1) and the disappearance of a small feature (Feature 3, which is a also σ^* feature). The transition underlying Feature 3 is to a large spatially extended state around the molecule in the gas phase; however, in the liquid, there are neighboring water molecules, interacting with the aromatic ring. Therefore, the disappearance of this feature is due directly to the ability of nearby water orbitals to mix with the relevant high-energy molecular orbitals, causing Feature 3 to disappear. This is likely Rydberg quenching or a similar phenomena.[13] In summary, our theoretical spectra correctly predict the subtle shift in feature locations and the disappearance of Feature 3 upon solvation, providing an encouraging benchmark for XAS theory.

Nitrogen K-edge

The experimental and theoretical calculations for the nitrogen K-edge of gas phase pyrrole are presented in Figure 5. This data was shown in a different format in previous work.[29] The calculated theoretical spectra are aligned to the experimental IP at 406.1 eV. The ISEELS data were taken previously, and are similar to the experimental NEXAFS vapor spectra.[14,16,17] The large first feature, Feature 1, has been assigned to a nitrogen 1s $\rightarrow$ 1π*(3b$_1$) feature. The second feature, Feature 2, has been variously assigned to a combination of transitions including those to the nitrogen 4p state and a variety of σ* features, including σ*(C-N) and σ*(C-H). The high energy resonance, Feature 3, at 412 eV has been assigned to a σ*(C-C) resonance.[14] Our calculated spectra are shown on the same figure, the dotted line depicting the spectra calculated with the fixed-nuclei approximation and the solid line depicting the spectra calculated with the average of 100 MD snapshots, with one standard deviation shaded. The first two features broaden and weaken in intensity by sampling a variety of snapshots. The first two features of the experimental spectrum are well reproduced in the gas phase calculations. We note that the second major feature is caused by a variety of resonance states, in agreement with previous assignments, which have large spatial extent. Unlike the carbon K-edge, the nitrogen K-edge spectrum is largely unaffected by the oligomerization of pyrrole. The flat dimer, trimer and polypyrrole spectra are similar to the monomer spectrum (not shown).

The spectra for pyrrole solvated in water are shown in Figure 6. The experimental spectra are taken at two different temperatures, ~295K and ~275K. It is worth noting that the spectra exhibit almost no change with temperature. The spectrum of pyrrole solvated in water was calculated, with the shaded error bar corresponding to one standard deviation over the 100

sampled snapshots. This calculation agrees well with experiment, accurately reproducing all three features.

The experimental liquid and gas phase spectra of the nitrogen K-edge exhibit features that remain largely unaltered upon being solvated by water. It is surprising that the orbitals appear to mix so little, particularly in light of the previous work on clusters, which predicted an effect similar to charge–transfer-to-solvent for the HOMO to LUMO transition.[9] A large spectral change is not observed in solvated pyrrole in the X-ray region, despite the nitrogen interacting with water. Upon solvation, the first feature red-shifts ~.3 eV and the FWHM broadens from 0.9 eV to 1.0 eV. The second major feature is largely unaffected by solvation, which is somewhat surprising, as this is a scattering feature and should be sensitive to molecular interactions. However, the geometry of the molecule could be largely unaffected by solvation and the energy of a scattering feature is largely dependent upon intramolecular bond lengths. It is possible the lack of feature movement could be a consequence, despite the large spatial extent of the scattering.[42] The third feature is also largely unaffected by solvation. A comparison to solid pyrrole is quite difficult due to low resolution at the nitrogen K-edge beyond mentioning that the three major features are still intact, meaning that in the solid the underlying states remain largely unchanged.[15] The alignment used in the case of the solid was merely to align the solid spectra with the gas spectra from the literature, so discussing relative feature shifts is impossible.[15] The overall background at high energy is larger in the solid, and the ratio of Feature 1 to Feature 2 is similar to what was calculated for the solution.

The theoretical calculations show changes between the condensed and gasoues spectra similar to what is found experimentally. If Feature 2 is used as the alignment between the computed and experimental spectra for solvated pyrrole, the first feature red shifts by .3 eV

upon condensing, and Feature 1 widens by .1 eV at FWHM, both identical to experiment. All the features lack the proper width, however, due to DFT's systematic underestimation of the bandwidth.[32]

While the carbons in pyrrole are somewhat hydrophobically solvated, the hydrogen bonded to the nitrogen should hydrogen bond with water. In our simulation, the mean distance between that hydrogen and the nearest oxygen of water is 2.34Å with a standard deviation of 0.36 Å. Although no new electronic transitions are introduced in the region of the first spectral feature at 402.4 eV, the interactions with water can cause this feature to shift in energy, explaining why the feature is so broad when pyrrole is solvated. This same effect also leads to the apparent red-shift. This antibonding orbital delocalizes to a small extent and hybridizes with the oribtals of nearby water molecules, which lowers the transition energy and due to conformational variations, broadens the feature. The second feature exhibits no change upon solvation, as predicted theoretically. Scattering features such as Feature 2 are believed to be highly sensitive to intramolecular distances, which should not change much upon solvation or temperature.[42]

Finally, we describe the orbital mixing between water and pyrrole. This leads in part to the decrease in intensity of Feature 1 observed upon solvation. The two transitions that contribute to Feature 1, the LUMO and LUMO+1, are separated by ~.02 eV in the gas phase. Shown in Figure 7 are the LUMO and LUMO+1 of pyrrole with a core hole on the nitrogen atom. . These are dramatically changed upon solvation. It appears in fact, that the bare LUMO + 1 corresponds to the solvated LUMO, and the solvated LUMO + 1 corresponds to the bare LUMO. The LUMO + 1 shows a particularly large amount of mixing with the waters. This lowers the intensity of this transition and therefore the intensity of the first feature relative to that

of the isolated molecule. The state exists on the nitrogen perpendicular to the nitrogen-hydrogen bond, as it must remain orthogonal to other states. In contrast, for the isolated molecule,, the LUMO extends out from the N-H into the vacuum. Hence, solvation does not alter the states enough to cause new spectral features to appear, but it does cause state reordering and the changing of spectral intensities.

4. Conclusions

The solvation of pyrrole by water was shown, perhaps surprisingly, to have only minor effects on the NEXAFS spectra, and hence on the electronic structure of this prototypical aromatic molecule. The nitrogen K-edge spectrum of pyrrole exhibits only slight changes with solvation in water when compared to the gas phase spectrum. There is a noticeable red-shifting of several features, as predicted by theoretical calculations, and attributed to interactions between the N-H group and the neighboring water molecules. The spectral features themselves remain largely intact, as found previously for the solid.

The carbon K-edge spectrum is complicated, resulting from two inequivalent carbon atoms and also being obscured by the oligomerization of pyrrole. The calculated gas phase spectrum generally has the correct form, although it underestimates the width of the prominent first feature. A shoulder on this feature is attributed to the oligomerization of pyrrole, which our calculations (as well as previous calculations) have been unable to reproduce, when considering only monomeric pyrrole. We investigate several candidate chemical species that contribute to this spectral feature and conclude that the fraction of carbons that have reacted is significant.

Generally excellent agreeement between our observed spectra and those calculated with the XCH method was found. This is an encouraging step in the search for a truly predictive theory of core-level spectra of complex molecules in solution.

Acknowledgements

Figure Captions

Figure 1. Experimental carbon K-edge NEXAFS (green) and ISEELS (red dotted) spectra of gaseous pyrrole with features labeled and a sketch of the molecular structure. The carbons are labeled 1 and 2 to differentiate between the calculated carbon spectra. The calculated carbon 1 fixed nuclei spectrum is shown (blue dots) with the classical MD overlaid (red with shaded error bars) and for carbon 2 the fixed nuclei spectra is shown (purple dots) with the classical MD overlaid (orange with error bars). The experimental ISEELS are from Ref. 19 and the calculated spectra are aligned to the experimental ionization potential of carbon 2 which is shown, as well as that of carbon 1. The calculated spectra are summed to give the total combined carbon K-edge spectra shown as summed fixed nuclei (orange dotted) and the summed MD spectra (purple). The arrows indicate corresponding features between theory and experiment.

Figure 2. Calculated carbon K-edge spectra of possible aggregation products are shown. The calculated nonbonded dimer spectrum is shown in blue. The structure of the chemically bonded dimer is shown at the top, and its calculated spectrum is shown in both the flat conformation (orange) and when twisted about the carbon-carbon bond formed upon dimerizing (red). The shoulder grows more intense for the trimer (green) and polypyrrole (yellow). The carbons labeled α give rise to the large subfeature also labeled α.

Figure 3. Experimental carbon K-edge NEXAFS (light green) and ISEELS (red dotted – from ref. 19) spectra of gaseous pyrrole. A 1:1 mixture of the flat pyrrole dimer and the pyrrole monomer (black) captures all the low energy features observed experimentally.

Figure 4. Experimental carbon K-edge NEXAFS of solvated pyrrole at ~295K (light green) and ~275 K (dark green) with features labeled and a drawing of the molecule. The carbons are labeled 1 and 2 to differentiate between the calculated carbon edges. The calculated carbon spectra are obtained from classical MD at 300K. The carbon 1 spectra are shown (blue with error bars) as are the carbon 2 spectra (red with error bars). The spectra are summed to give the total combined carbon K-edge spectrum (purple).

Figure 5. Experimental nitrogen K-edge NEXAFS (green) and ISEELS (red dotted) spectra of gaseous pyrrole and calculated fixed nuclei (purple dashed) and classical MD (blue with error bars) spectra of pyrrole with features labeled and the molecule studied pictured. The average spectrum for classical MD are shown in darker colors, and one standard deviation is shown as a lightly shaded line for the classical MD spectra. The experimental ionization potential is shown as a vertical line. The experimental ISEELS is from ref 19.

Figure 6. Experimental nitrogen K-edge NEXAFS spectra of pyrrole solvated in water at ~295 K (orange) and ~275 K (yellow) and a calculated spectrum at 300K of the solvated molecule from classical MD (green with error bars) with features labeled. The average spectrum for classical MD are shown in darker colors, with one standard deviation lightly shaded.

Figure 7. Isosurfaces are shown for the LUMO and LUMO+1 of the excited state of pyrrole with and without water, corresponding to 30% of the total integrated value. The nitrogen atom is at the top of the pyrrole molecule in each of these images. These are the transitions that cause the intense first feature of the nitrogen K-edge of pyrrole. Part of the reason the state decreases

in intensity upon solvation is due to the mixing of the LUMO+1 with the surrounding water

molecules greatly lowering this transitions intensity. Such mixing is not as strong in the case of

the LUMO.
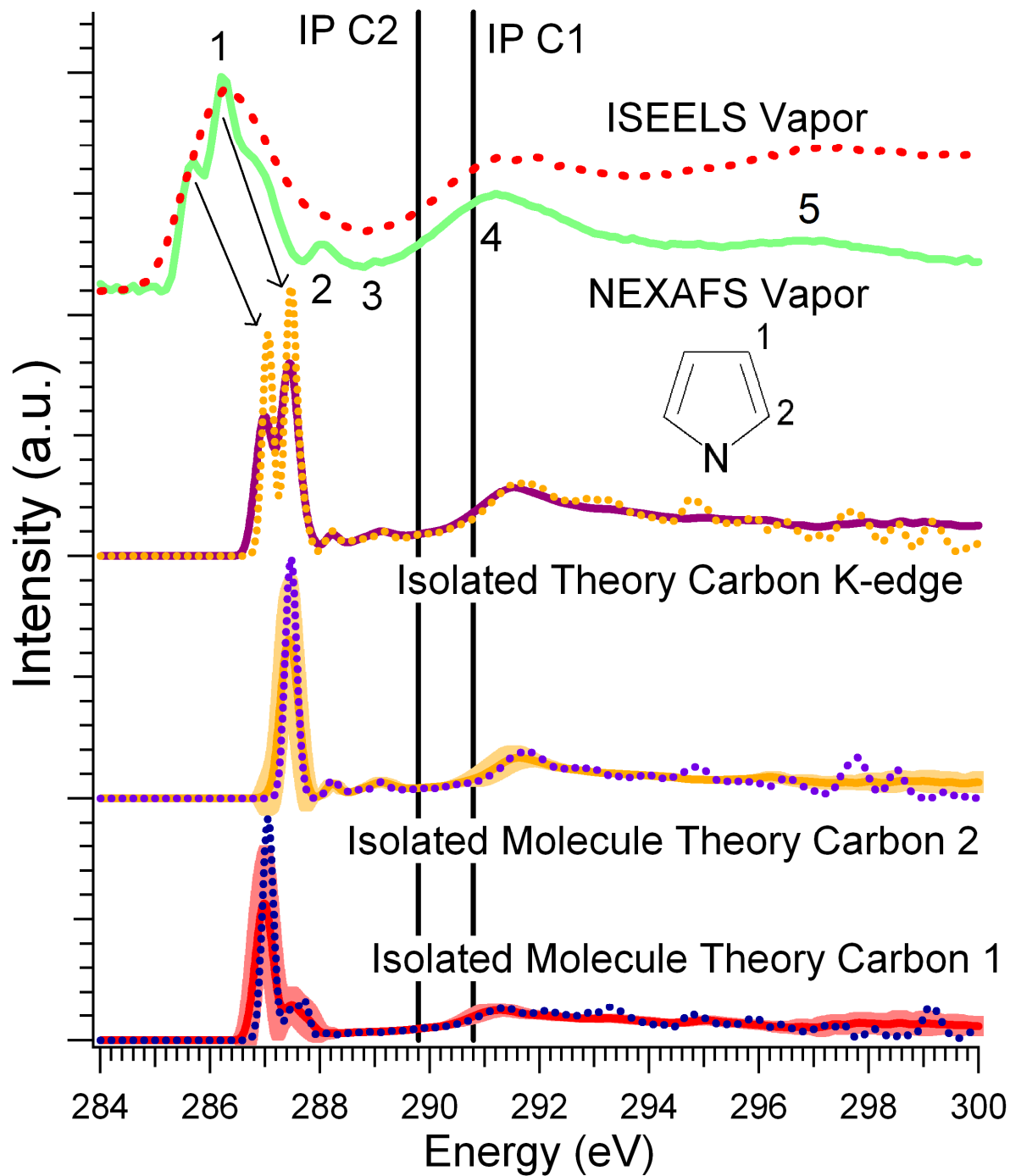
Figure 1
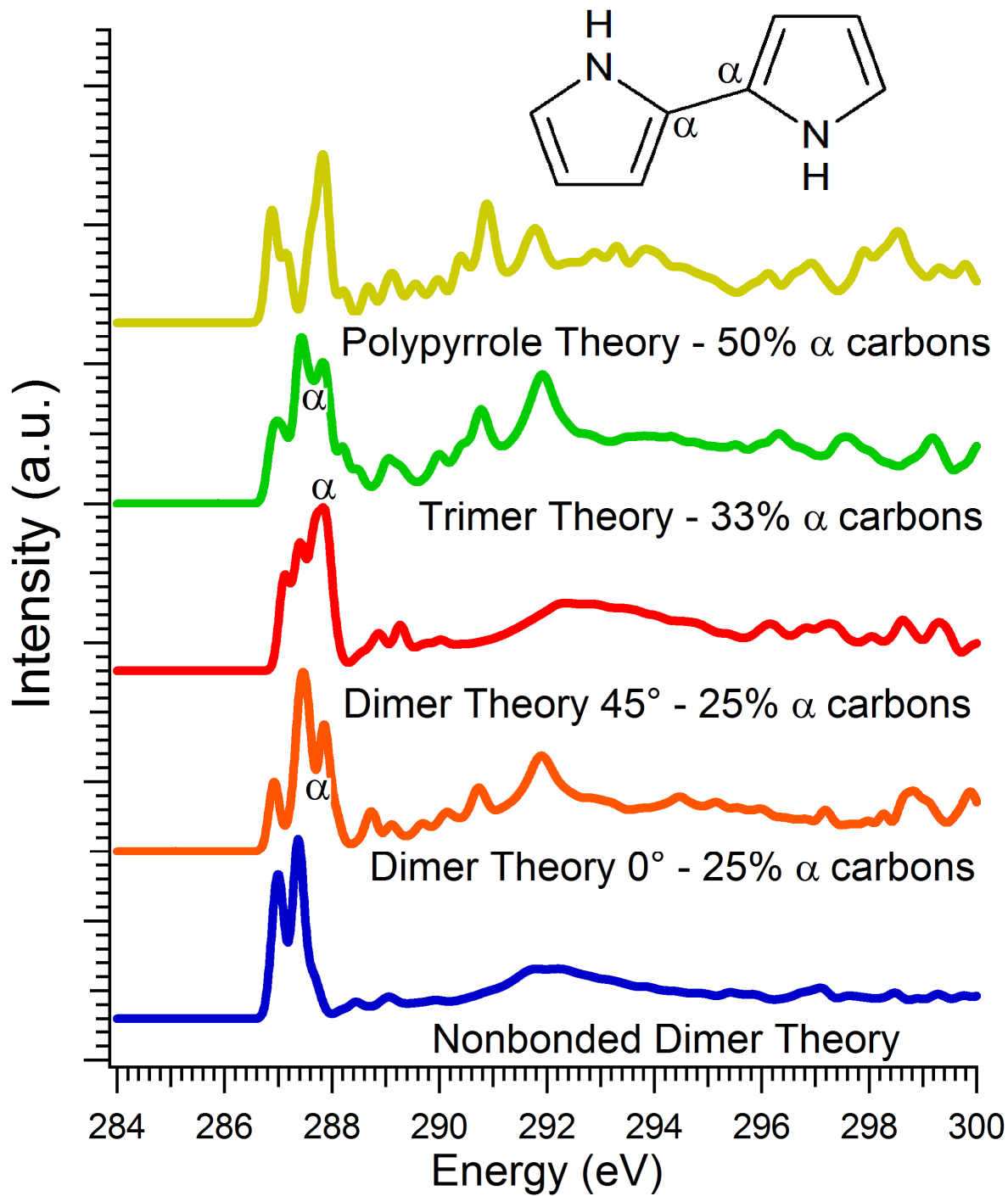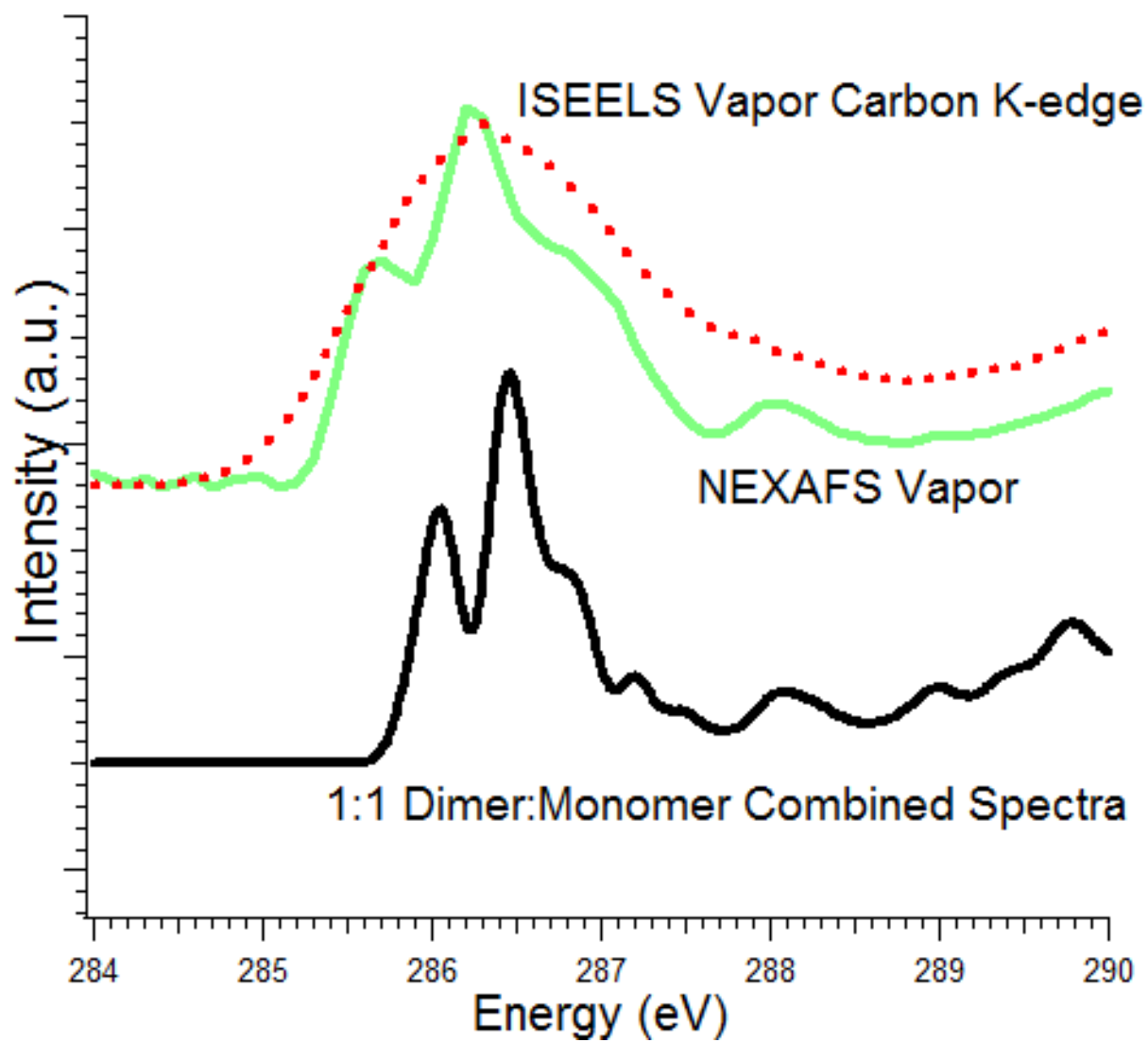
Figure 2

Figure 3
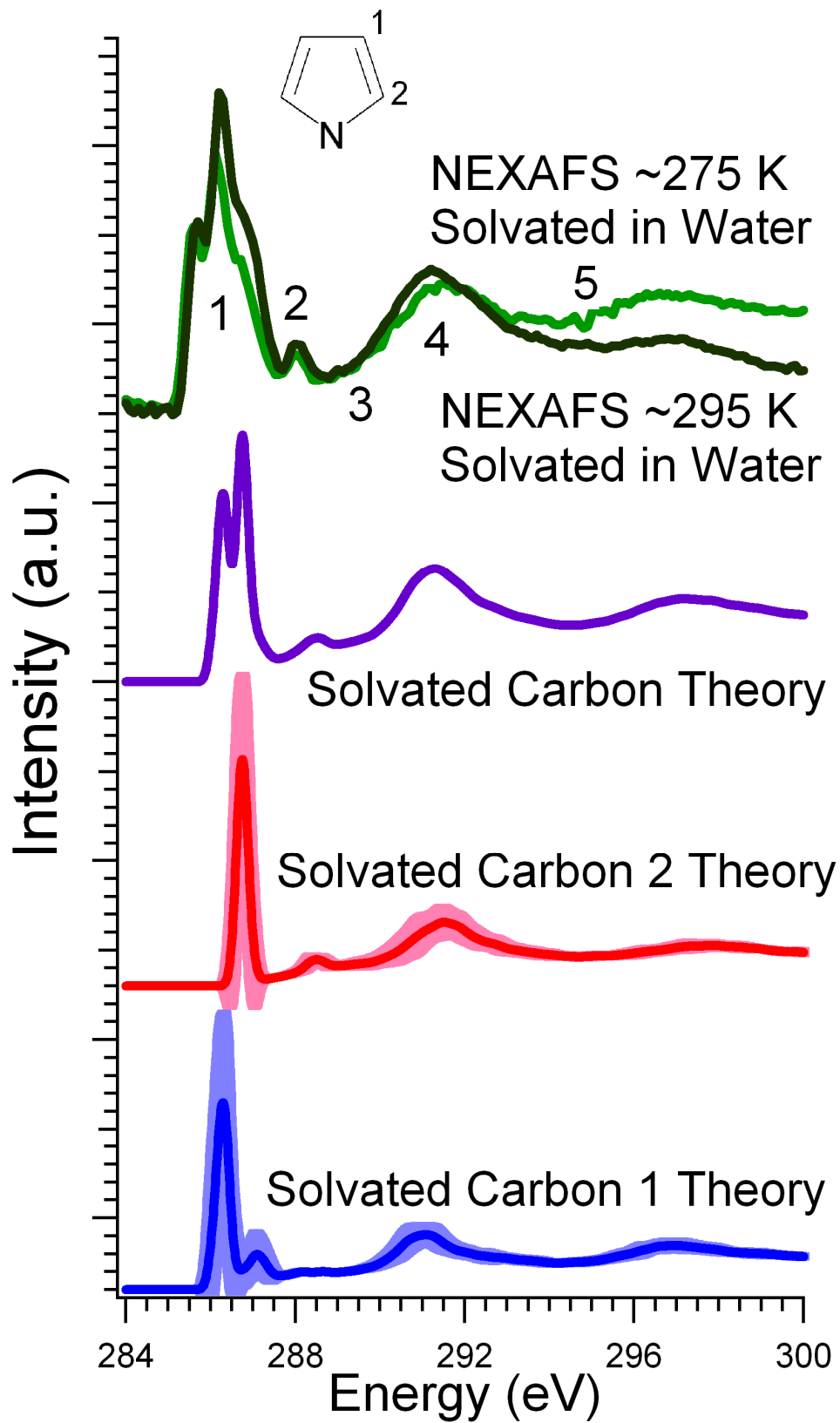
Figure 4

Figure 5

Figure 6

	LUMO	LUMO + 1
Solvated		
Bare		
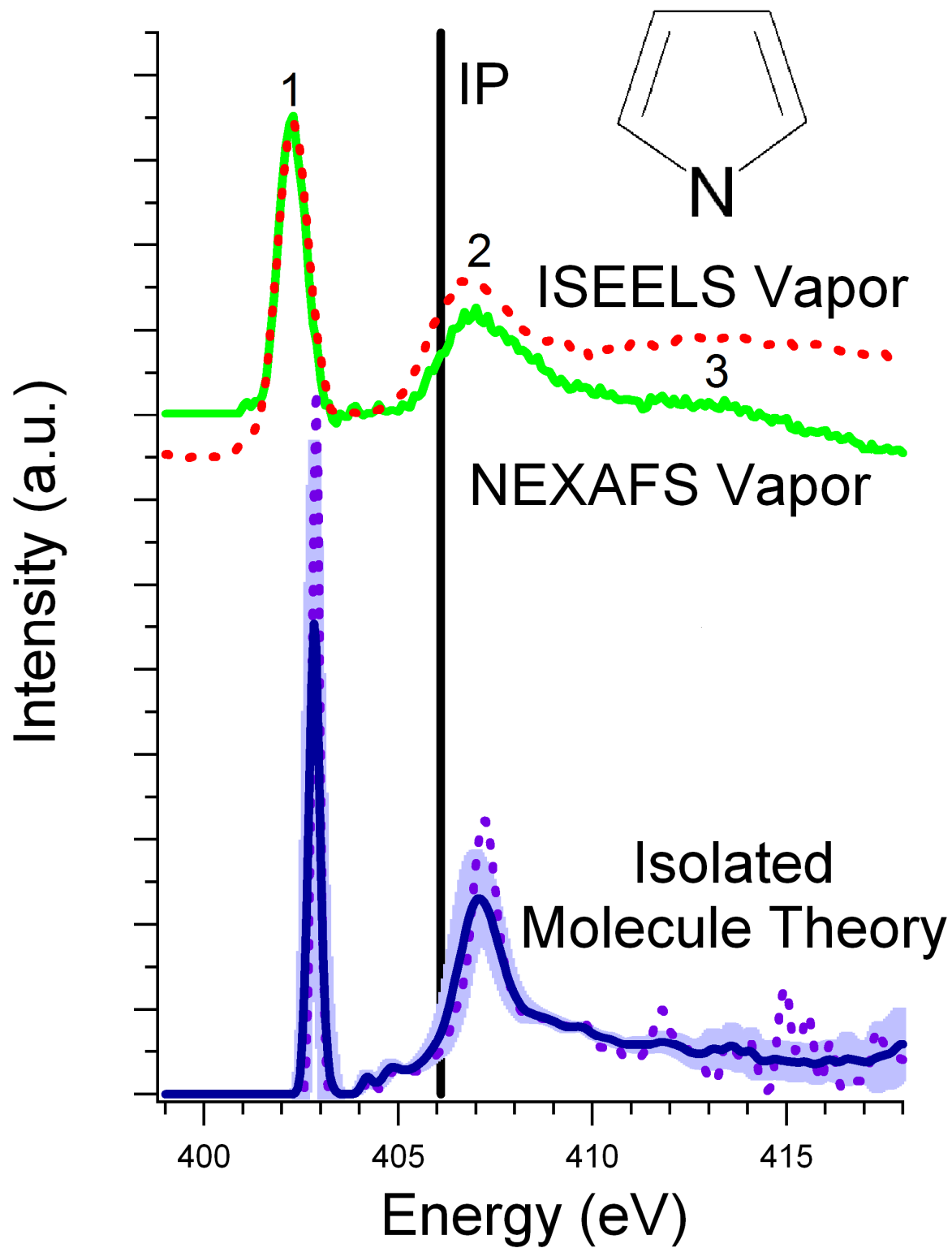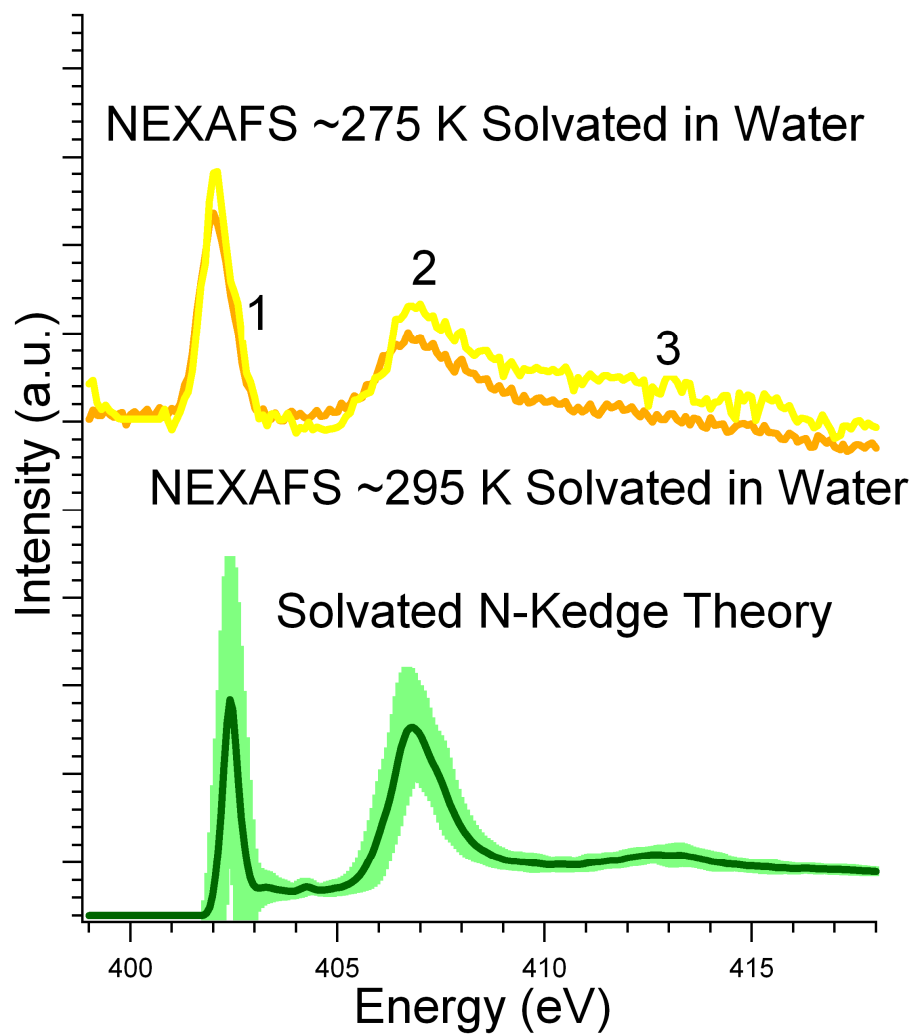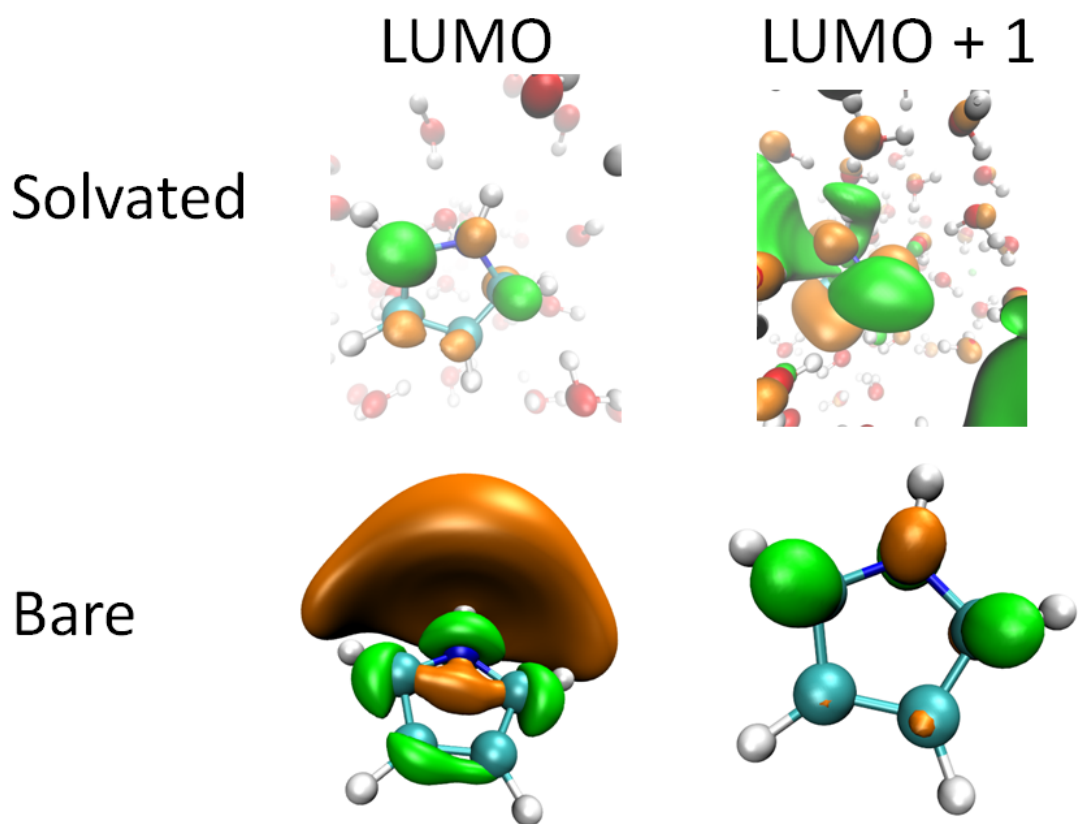
Figure 7

1   D. R. Lide, *CRC Handbook of Chemistry and Physics, 88th Edition*. (CRC, 2007).

2   R. H. Linnell and S. Umar, Archives of Biochemistry and Biophysics **57** (1), 264 (1955);

       A. Stolarz and J. Szydlowski, Journal of Radioanalytical and Nuclear Chemistry-Articles

       185 (2), 219 (1994).

3   B. M. Messer, C. D. Cappa, J. D. Smith, K. R. Wilson, M. K. Gilles, R. C. Cohen, and R.

       J. Saykally, Journal of Physical Chemistry B **109** (11), 5375 (2005).

4   E. F. Aziz, N. Ottosson, M. Faubel, I. V. Hertel, and B. Winter, Nature **455** (7209), 89

       (2008); J. S. Uejio, C. P. Schwartz, A. M. Duffin, W. S. Drisdell, R. C. Cohen, and R. J.

       Saykally, Proceedings of the National Academy of Sciences of the United States of

       America **105** (19), 6809 (2008).

5   K. R. Wilson, B. S. Rude, T. Catalano, R. D. Schaller, J. G. Tobin, D. T. Co, and R. J.

       Saykally, Journal of Physical Chemistry B **105** (17), 3346 (2001).

6   P. Parent, C. Laffon, C. Mangeney, F. Bournel, and M. Tronc, Journal of Chemical

       Physics **117** (23), 10842 (2002).

7   G. Vall-llosera, B. Gao, A. Kivimaeki, M. Coreno, J. A. Ruiz, M. de Simone, H. Agren,

       and E. Rachlew, Journal of Chemical Physics **128** (4) (2008); Y. Zubavichus, M.

       Zharnikov, A. Schaporenko, and M. Grunze, Journal of Electron Spectroscopy and

       Related Phenomena **134** (1), 25 (2004).

8   M. J. Tubergen, A. M. Andrews, and R. L. Kuczkowski, Journal of Physical Chemistry

       97 (29), 7451 (1993); M. A. Martoprawiro and G. B. Bacskay, Molecular Physics **85** (3),

       573 (1995).

9   A. L. Sobolewski and W. Domcke, Chemical Physics Letters **321** (5-6), 479 (2000).

[10] P. Tuomikoski, Journal of Chemical Physics **20** (6), 1054 (1952).

[11] D. Chandler, Nature **437** (7059), 640 (2005); L. R. Pratt, Annual Review of Physical Chemistry **53**, 409 (2002).

[12] H. S. Ashbaugh and L. R. Pratt, Reviews of Modern Physics **78** (1), 159 (2006).

[13] E. Otero and S. G. Urquhart, Journal of Physical Chemistry A **110** (44), 12121 (2006).

[14] D. C. Newbury, I. Ishii, and A. P. Hitchcock, Canadian Journal of Chemistry-Revue Canadienne De Chimie **64** (6), 1145 (1986).

[15] M. Mauerer, P. Zebisch, M. Weinelt, and H. P. Steinruck, Journal of Chemical Physics **99** (5), 3343 (1993).

[16] C. Hennig, K. H. Hallmeier, A. Bach, S. Bender, R. Franke, J. Hormes, and R. Szargan, Spectrochimica Acta Part a-Molecular and Biomolecular Spectroscopy **52** (9), 1079 (1996).

[17] D. Duflot, C. Hannay, J. P. Flament, and M. J. Hubin-Franskin, Journal of Chemical Physics **109** (13), 5308 (1998).

[18] I. Dauster, C. A. Rice, P. Zielke, and M. A. Suhm, Physical Chemistry Chemical Physics **10** (19), 2827 (2008).

[19] M. F. Suarez-Herrera and J. M. Feliu, Physical Chemistry Chemical Physics **10** (46), 7022 (2008).

[20] Y. C. Liu, S. J. Yang, T. C. Chuang, and C. C. Wang, Journal of Electroanalytical Chemistry **570** (1), 1 (2004).

[21] F. Beck, M. Oberst, and R. Jansen, Electrochimica Acta **35** (11-12), 1841 (1990).

[22] M. Aoki, A. Ishihara, and T. Kabe, Nippon Kagaku Kaishi (1), 57 (1991).

23   K. R. Wilson, B. S. Rude, J. Smith, C. Cappa, D. T. Co, R. D. Schaller, M. Larsson, T. Catalano, and R. J. Saykally, Review of Scientific Instruments **75** (3), 725 (2004).

24   J. D. Smith, C. D. Cappa, W. S. Drisdell, R. C. Cohen, and R. J. Saykally, Journal of the American Chemical Society **128** (39), 12892 (2006).

25   P. Hohenberg and W. Kohn, Physical Review B **136** (3B), B864 (1964); W. Kohn and L. J. Sham, Physical Review **140** (4A), 1133 (1965); J. P. Perdew, J. A. Chevary, S. H. Vosko, K. A. Jackson, M. R. Pederson, D. J. Singh, and C. Fiolhais, Physical Review B **46** (11), 6671 (1992).

26   C. Kolczewski, R. Puttner, O. Plashkevych, H. Agren, V. Staemmler, M. Martins, G. Snell, A. S. Schlachter, M. Sant'Anna, G. Kaindl, and L. G. M. Pettersson, Journal of Chemical Physics **115** (14), 6426 (2001).

27   L. G. M. Pettersson, T. Hatsui, and N. Kosugi, Chemical Physics Letters **311** (3-4), 299 (1999); J. J. Rehr, Radiation Physics and Chemistry **75** (11), 1547 (2006); A. Nilsson and L. G. M. Pettersson, Surface Science Reports **55** (2-5), 49 (2004).

28   U. Ekstrom and P. Norman, Physical Review A **74** (4) (2006).

29   J. S. Uejio, C. P. Schwartz, R. J. Saykally, and D. Prendergast, Chemical Physics Letters **467** (1-3), 195 (2008).

30   D. Prendergast and G. Galli, Physical Review Letters **96** (21) (2006).

31   D. Prendergast, J. C. Grossman, and G. Galli, Journal of Chemical Physics **123** (1) (2005).

32   C. P. Schwartz, J. S. Uejio, R. J. Saykally, and D. Prendergast, The Journal of Chemical Physics **130** (18), 184109 (2009).

33   J. S. Uejio, C. P. Schwartz, A. M. Duffin, A. H. England, R. J. Saykally, and D. Prendergast, Journal of the American Chemical Society **Submitted** (2009).

34   D. K. Singh, S. K. Srivastava, A. K. Ojha, and B. P. Asthana, Spectrochimica Acta Part a-Molecular and Biomolecular Spectroscopy **71** (3), 823 (2008).

35   S. Baroni, A. D. Corso, S. D. Gironcoli, and P. Giannozzi, PWSCF (2008).

36   J. P. Perdew, K. Burke, and M. Ernzerhof, Physical Review Letters **77** (18), 3865 (1996).

37   G. Herzberg and E. Teller, Zeitschrift Fur Physikalische Chemie-Abteilung B-Chemie Der Elementarprozesse Aufbau Der Materie **21** (5/6), 410 (1933).

38   T. A. D. D.A. Case, T.E. Cheatham, III, C.L. Simmerling, J. Wang, R.E. Duke, R., K. M. M. Luo, D.A. Pearlman, M. Crowley, R.C. Walker, W. Zhang, B. Wang, S., A. R. Hayik, G. Seabra, K.F. Wong, F. Paesani, X. Wu, S. Brozell, V. Tsui, H., L. Y. Gohlke, C. Tan, J. Mongan, V. Hornak, G. Cui, P. Beroza, D.H. Mathews, C., and W. S. R. Schafmeister, and P.A. Kollman, (2006); J. M. Wang, W. Wang, P. A. Kollman, and D. A. Case, Journal of Molecular Graphics & Modelling **25** (2), 247 (2006).

39   L. A. Naslund, D. C. Edwards, P. Wernet, U. Bergmann, H. Ogasawara, L. G. M. Pettersson, S. Myneni, and A. Nilsson, Journal of Physical Chemistry A **109** (27), 5995 (2005).

40   D. Duflot, J. P. Flament, A. Giuliani, J. Heinesch, and M. J. Hubin-Franskin, Journal of Chemical Physics **119** (17), 8946 (2003).

41   G. Columberg and A. Bauder, Journal of Chemical Physics **106** (2), 504 (1997).

42   J. Stöhr, *NEXAFS Spectroscopy*. (Springer, Berlin, 1992).